nature communications

Article

https://doi.org/10.1038/s41467-024-52676-w

Electrically switchable 2^N-channel wave-front control for certain functionalities with N cascaded polarization-dependent metasurfaces

Received: 4 June 2024

Accepted: 13 September 2024

Published online: 27 September 2024

Check for updates

Zhiyao Ma, Tian Tian, Yuxuan Liao, Xue Feng ✉, Yongzhuo Li, Kaiyu Cui, Fang Liu, Hao Sun, Wei Zhang & Yidong Huang ✉

Metasurfaces with tunable functionalities are greatly desired for modern optical system and various applications. To increase the operating channels of polarization-multiplexed metasurfaces, we proposed a structure of N cascaded dual-channel metasurfaces to achieve 2^N electrically switchable channels without intrinsic loss or cross-talk for certain functionalities, including beam steering, vortex beam generation, lens, etc. As proof of principles, we have implemented a 3-layer setup to achieve 8 channels. In success, we have demonstrated two typical functionalities of vortex beam generation with switchable topological charge of $l = -3 \sim +4$ or $l = -1 \sim -8$, and beam steering with the deflection direction switchable in an 8×1 line or a 4×2 grid. We believe that our proposal would provide a practical way to significantly increase the scalability and extend the functionality of polarization-multiplexed metasurfaces. Although this method is not universal, it is potential for the applications of LiDAR, glasses-free 3D display, OAM (de)multiplexing, and varifocal meta-lens.

Metasurfaces[1,2] arouse broad research interest due to the unprecedented manipulation of lightwave in terms of phase[1,2], amplitude[3–5], polarization[6,7], and frequency[8,9]. Metasurfaces possess rich advantages over traditional planar optical devices, including compact footprint and thickness[10,11], subwavelength-resolution control of lightwave[7,12,13], low-loss tramsmition[14] as well as versatile functionalities[15,16]. In particular, with the abrupt phase-shifting ability in subwavelength scale[1], metasurfaces have gained significant progress in the fixed wave-front controlling, e.g., beam steering[17,18], meta-lens[19,20], vortex beam generation[4,6,21], holograms[22,23], etc. With the growing need of optical systems, metasurfaces with tunable functionalities are further concerned. One approach is dynamically reconfiguring the subwavelength structure by various mechanisms, including electro-optic[24–27], mechanical[28–30], phase transition[31,32], etc. Thus, the response of the metasurface can be tuned with reconfiguring structure. However, there are remaining technical challenges for reconfigurable metasurfaces. On the one hand, the available functionalities would be limited for mechanisms like phase-transition[31,32] and mechanical stretching[28–30]. On the other hand, to reconfigure a metasurface pixel-by-pixel by electro-optical mechanism[24–27], the extra complexity would significantly affect the scalability and increase the cost, i.e., the numerous electrodes. Another approach depends on the states of input lightwave, which serve as knobs for tuning the response of fixed metasurfaces[33], thus tuning the functionalities in success. The properties include incident angle[34,35] or direction[36,37], wavelength[38–41], carried orbital angular momentum (OAM)[42,43]. Besides, with two cascaded metasurfaces, the functionalities can be also tuned by the relative displacement[44–46] and rotation[47,48]. Actually, with these methods, the input lightwave at the second metasurface is manipulated equivalently, while the structures of both metasurfaces are fixed.

Department of Electronic Engineering, Tsinghua University, Beijing, China. ✉e-mail: x-feng@tsinghua.edu.cn; yidonghuang@tsinghua.edu.cn

As an intrinsic property of lightwave, polarization has been used for tuning the response of metasurfaces as well, which is also regarded as polarization multiplexing[49–53]. Polarization multiplexing can be achieved by employing polarization-dependent subwavelength structures, without compromising on resolution and information capacity of metasurfaces[52]. For such polarization-dependent metasurfaces, the functionalities can be independently designed for two orthogonal polarization states of input light, e.g., horizontal and vertical linear polarization[51]. As for specific functionalities, dual-channel lenses[49,54], dual-channel holograms[51], and dual-channel vortex beam generators[50,55] have been achieved. Since the degrees of freedom (DoFs) of polarization state is only two, the number of independent channels is also limited to two for a single metasurface. This limitation can be broken by employing a polarizer after the metasurface, so that the off-diagonal elements of the Jones matrix can be extracted as the third independent channel[56]. Furthermore, engineered noise have been employed to increase the number of channels up to 11 with moderate cross-talk[57]. These approaches significantly increased the scalability of polarization-multiplexed metasurfaces. However, there would be intrinsic loss and additional design complexity since the required Jones matrices are non-unitary[56,57]. Besides, although the introduced cross-talk is moderate in holograms, it would be unacceptable in noise-sensitive or cross-talk-sensitive applications, e.g., OAM (de)multiplexing, LiDAR. Generally, the independent channels without intrinsic cross-talk are still limited to three. Therefore, it is still challenging for further increasing channels and extending the functionality of polarization-multiplexed metasurfaces.

In this work, we propose a practical approach to increase the number of channels to 2^N for certain functionalities without intrinsic loss or cross-talk by cascading N metasurfaces. To increase the DoFs on polarization, a direct consideration is to cascade multiple polarization-dependent metasurfaces. Cascading N metasurfaces combined with polarization controllers would increase the total DoFs of polarization up to $N+1$, which would be further discussed in the section of "Results". Obviously, the cost of cascading N metasurfaces would be too high if the number of the obtained channels is only $N+1$. However, we found that the channels can be increase to 2^N under certain condition. The condition is that the phase pattern of cascaded structure should have the same function form with that of a single metasurface, while the parameters of the cascaded structure are summation of each single metasurface. Such condition could be satisfied in some common functionalities, including beam steering, vortex beam generation, lens, etc. Thus, the channels of polarization-multiplexing can be increased exponentially for certain dynamic wave-front controlled functionalities and applications. As proof of principle, we have implemented an 8-channel setup through cascading 3 layers of metasurfaces. Thus, 8-channel vortex beam generation as well as beam steering have been experimentally demonstrated and characterized, respectively. In vortex beam generation, the topological charge (TC, denoted as l) can be switched within the range of $l=-3$ to $+4$ or $l=-1$ to -8, and the total transmittance of $l=-3$ to $+4$ is within the range from 31.6% to 33.7%. While in beam steering, the deflection direction can be switched in an 8×1 line or a 4×2 grid, and the total transmittance is within the range from 15% to 25%. Besides, since the employed polarization controllers are electrically tunable liquid crystal (LC) phase retarders, the structure can be electrically switched among different channels.

Results

Pincple

Based on a polarization-dependent metasurface, two independent phase-only patterns can be designed to modulate on the wave-front of the input lightwave with two orthogonal polarization states respectively. Such two phase patterns correspond to two functional channels so that dual-channel switchable wave-front control can be achieved. Since the DoFs of polarization state is only two, there are only two independent functional channels of a single polarization-dependent metasurface in theory. To increase the number of channels, our proposal is to cascade N dual-channel metasurfaces, while setting N polarization controllers before each metasurface as shown in Fig. 1a. Without loss of generality, suppose the pre-settled orthogonal polarization states of input light of each metasurface are horizontal and vertical linear polarization, denoted as $|H\rangle$ and $|V\rangle$. It should be mentioned that the employed orthogonal states can be another set, e.g., left-hand and right-hand circular polarization[50,55]. The polarization controllers are employed to switch the polarization state of input light at each metasurface between $|H\rangle$ and $|V\rangle$. As a result, for each metasurface, one of the two designed phase patterns is picked up. Thus, in the whole structure, there would be 2^N combinations of cascaded phase patterns. Suppose the dual phase patterns of the i-th metasurface are $\varphi_{H,i}(x,y)$ and $\varphi_{V,i}(x,y)$, the equivalent phase pattern of the whole structure can be expressed by the summation of the selected phase pattern from each metasurface:

$$\varphi_{\boldsymbol{\mu}}(x,y)=\sum_{i=1}^{N}\varphi_{\mu_i,i}(x,y)$$

$$\begin{bmatrix}\varphi_{[H,H,\ldots,H]^{\mathrm{T}}}\\ \varphi_{[V,H,\ldots,H]^{\mathrm{T}}}\\ \vdots\\ \varphi_{[V,V,\ldots,V]^{\mathrm{T}}}\end{bmatrix}_{2^N\times1}=\begin{bmatrix}1&0&1&0&\cdots&1&0\\ 0&1&1&0&\cdots&1&0\\ \vdots&\vdots&\vdots&\vdots&\ddots&\vdots&\vdots\\ 0&1&0&1&\cdots&0&1\end{bmatrix}_{2^N\times2N}\begin{bmatrix}\varphi_{H,1}\\ \varphi_{V,1}\\ \varphi_{H,2}\\ \varphi_{V,2}\\ \vdots\\ \varphi_{H,N}\\ \varphi_{V,N}\end{bmatrix}_{2N\times1} \tag{1}$$

Where $\boldsymbol{\mu}$ is a $N\times1$ vector representing input polarization states of each metasurface. Since μ_i is either H or V and determined by the i-th polarization controller, $\boldsymbol{\mu}$ can take 2^N distinct values. For more clarity, the matrix-vector multiplication form is expanded in the second line of Eq. 1. It should be mentioned that in the coefficient matrix, the summation of the $2m-1$ column and the $2m$ column for any integer $m\le N$ is always a column vector with all elements of 1, thus the rank of the matrix is actually $N+1$. That is to say, the number of independent channels is constrained to $N+1$ in general, although there are 2^N cascaded phase patterns.

Here, the concept of independence should be discussed in details. The number of combinations for the cascaded phase pattern is still 2^N, but there would be correlation among them. Thus, these 2^N cascaded phase patterns are not independent, as well as the corresponding functionalities. In other words, only $N+1$ among the 2^N cascaded phase patterns can be arbitrarily or independently designed, while the others would be determined by them. This corollary is mentioned in the section of "Introduction".

However, under certain conditions, it would be possible to achieve 2^N channels with distinct functionalities. The condition is that phase pattern of cascaded structure should have the same function form with that of a single metasurface, while the parameters of the cascaded structure are summation of each single metasurface. To be more specific, for some common functionalities, the target of wave-front control is to manipulate certain parameters of the light field. For such a functionality, suppose the form of the phase pattern can be written as $\varphi_{\mathrm{F}}(x,y,p^{(1)},p^{(2)},\ldots)$, which is a map of the target parameters $p^{(1)}$, $p^{(2)}$, ... If we consider a functionality, in which φ_{F} is a linear map of these target parameters, the equivalent phase pattern of multiple cascaded metasurfaces with such functionality can be rewritten as:

$$\sum_{i=1}^{N}\varphi_{\mathrm{F}}\left(x,y,p_i^{(1)},p_i^{(2)},\ldots\right)=\varphi_{\mathrm{F}}\left(x,y,\sum_{i=1}^{N}p_i^{(1)},\sum_{i=1}^{N}p_i^{(2)},\ldots\right) \tag{2}$$

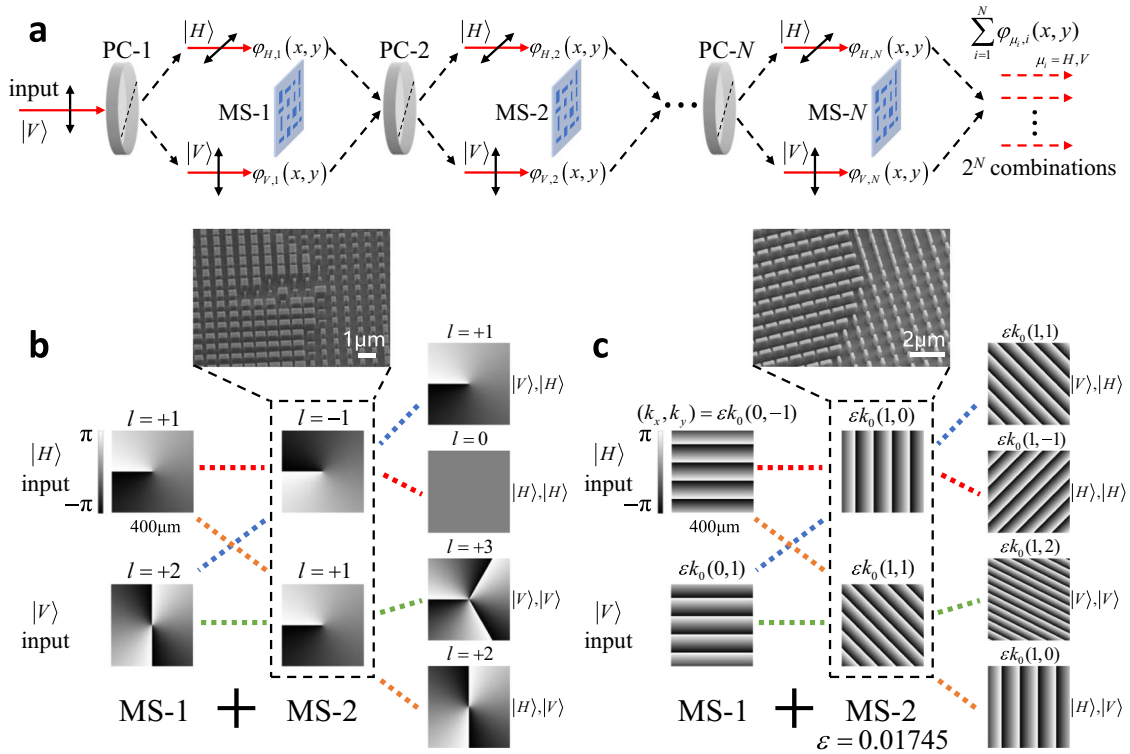

Fig. 1 | Principle of 2^N-channel switchable wave-front control for certain functionalities. a The schematic of the cascaded structure. *N* polarization-dependent dual-channel metasurfaces (MSs) are cascaded. The initial input state is $|V\rangle$. A polarization controller (PC) is set before each metasurface to switch the input state at each metasurface between $|H\rangle$ and $|V\rangle$, thus one of the dual phase patterns is picked up. The whole phase pattern would be the summation of all picked phase patterns. **b** Example of cascading two dual-channel vortex phase patterns to generate four channels of vortex phase patterns. The TCs of the first pattern are $l = +1$, +2 for $|H\rangle$ and $|V\rangle$ input, respectively. While the TCs of the second pattern are $l = -1$, +1, with the inset of a SEM image of the corresponding metasurface. The TCs of four cascaded channels are $l = +1$, 0, +3, +2. **c** Example of cascading two dual-channel blazed grating patterns to generate four channels of blazed grating patterns. The momenta of the first pattern are $(k_x,k_y) = \varepsilon k_0(0,-1)$, $\varepsilon k_0(0,1)$ for $|H\rangle$ and $|V\rangle$ input, respectively. While the TCs of the second pattern are $(k_x,k_y) = \varepsilon k_0(1,0)$,$\varepsilon k_0(1,1)$, with the inset of a SEM image of the corresponding metasurface. The momenta of four cascaded channels are $(k_x,k_y) = \varepsilon k_0(1,1)$,$\varepsilon k_0(1,-1)$,$\varepsilon k_0(1,2)$,$\varepsilon k_0(1,0)$. Where k_0 is the absolute value of wavevector in vacuum, $\varepsilon = 0.01745$ is a constant.

As seen in Eq. 2, the equivalent phase pattern can be rewritten from cascaded phase patterns into a set of cascaded parameters $\sum_{i=1}^{N} p_i^{(1)}, \sum_{i=1}^{N} p_i^{(2)}, \ldots$, which is still in the form of φ_F. Thus, the equivalent functionality of cascaded metasurfaces would be as same as a single metasurface, while the parameters are modified.

It should be mentioned that the number of target parameters is determined by the functionality. Specifically, there are several examples of functionalities with such linear-map property. For the functionality of vortex beam generation, the required vortex phase pattern can be written as $\varphi_{OAM}(x,y,l) = l \cdot \arctan2(y,x)$[58]. Obviously, the phase pattern is a linear map of a single target parameter that is the TC *l*. As seen in Eq. 3, cascading vortex phase patterns is equivalent to a vortex phase pattern as well. The cascaded TC would be the summation of TCs of each single pattern. For the functionality of beam steering, the required phase patterns are blazed grating patterns with $\varphi_{BG}(x,y,k_x,k_y) = k_x x + k_y y$[59]. Here, the phase pattern is a linear map of two target parameters, which are the transverse momenta k_x and k_y, respectively. As seen in Eq. 4, cascading blazed grating patterns is equivalent to a blazed grating pattern as well. The cascaded momenta would be the summation of momenta of each single pattern.

$$\sum_{i=1}^{N} \varphi_{OAM}(x,y,l_i) = \sum_{i=1}^{N} (l_i \cdot \arctan2(y,x)) = \arctan2(y,x) \cdot \left(\sum_{i=1}^{N} l_i \right) \quad (3)$$

$$\sum_{i=1}^{N} \varphi_{BG}(x,y,k_{x,i},k_{y,i}) = \sum_{i=1}^{N} (k_{x,i}x + k_{y,i}y) = x \sum_{i=1}^{N} (k_{x,i}) + y \sum_{i=1}^{N} (k_{y,i}) \quad (4)$$

Besides, for the functionality of lens, the required phase pattern can be written as a linear-map of the reciprocal focal length[60] as well. However, the functionality of hologram is a counter-example, where the required phase pattern is usually numerically calculated and cannot be written as a linear map of explicit parameters. Thus, the equivalent functionality of multiple cascaded holograms cannot guarantee a meaningful hologram.

Combining the linear-map property (Eq. 2) with the cascaded polarization-dependent metasurfaces, 2^N functional channels can be achieved as shown in Fig. 1a. Here, the dual phase patterns of each single metasurface in Eq. 1 should be determined by the mapping relation φ_F and corresponding target parameters. For the *i*-th polarization-dependent metasurface, suppose the parameters of the phase pattern for input polarization state $|H\rangle$ are $p_{H,i}^{(1)}, p_{H,i}^{(2)}, \ldots$, while the parameters for $|V\rangle$ are $p_{V,i}^{(1)}, p_{V,i}^{(2)}, \ldots$. Then the phase patterns of the *i*-th metasurface can be rewritten as:

$$\begin{aligned} \varphi_{H,i}(x,y) &= \varphi_F\left(x,y,p_{H,i}^{(1)},p_{V,i}^{(2)},\ldots\right) \\ \varphi_{V,i}(x,y) &= \varphi_F\left(x,y,p_{H,i}^{(1)},p_{V,i}^{(2)},\ldots\right) \end{aligned} \quad (5)$$

To write the cascaded phase patterns, substitute $\varphi_{H,i}$'s and $\varphi_{V,i}$'s in Eq. 1 with Eq. 5, and apply the linear-map property in Eq. 2:

$$\varphi_{\boldsymbol{\mu}}(x,y) = \sum_{i=1}^{N} \varphi_F\left(x,y,p_{\mu_i,i}^{(1)},p_{\mu_i,i}^{(2)},\ldots\right) = \varphi_F\left(x,y,\sum_{i=1}^{N} p_{\mu_i,i}^{(1)},\sum_{i=1}^{N} p_{\mu_i,i}^{(2)},\ldots\right) \quad (6)$$

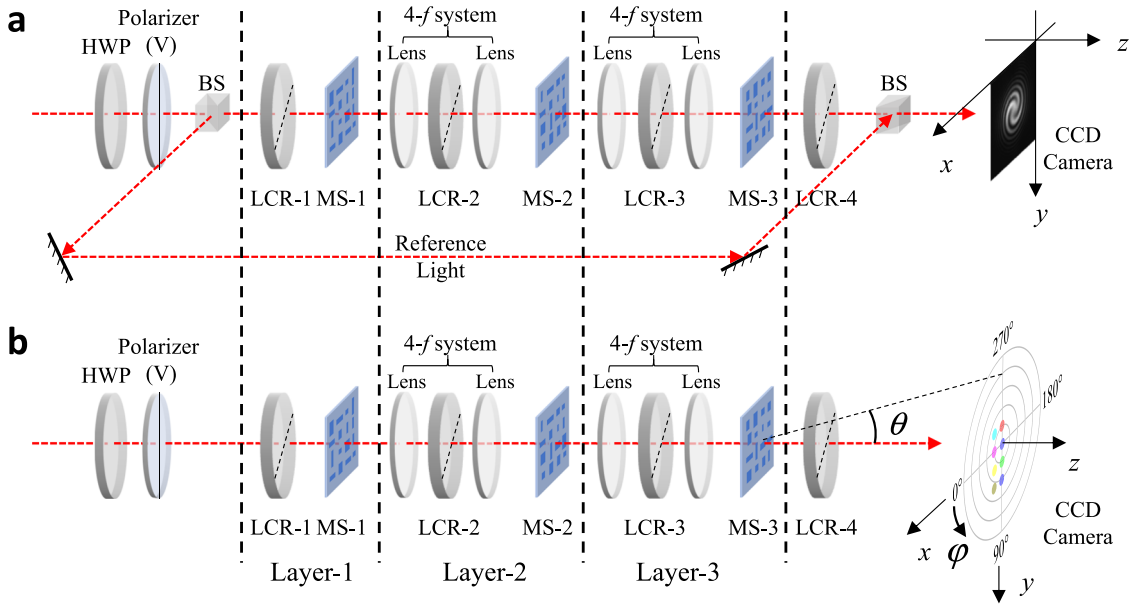

Fig. 2 | Implementation of 8-channel switchable wave-front control for certain functionalities with 3-layer setup. The input fundamental Gaussian beam is filtered into polarization state $|V\rangle$. Liquid crystal retarders (LCR) with slow axis at 45° are utilized as polarization controllers. The 4-*f* systems are employed to guarantee the cascaded phase pattern is simply the summation of each single phase pattern, without considering the propagation between metasurfaces (MSs). LCR-4 is employed to switch the output polarization state back to $|V\rangle$. **a** In the characterization of TCs of generated vortex beam, a path of reference light is employed for the interference fringes. An example of interference fringe with $l = -2$ is show on the right. **b** In the characterization of beam steering, the deflection direction is characterized with θ and φ in spherical coordinates. An example of distribution of 8 deflection directions is show on the right.

As seen in Eq. 6, for 2^N combinations of input polarization states, all the 2^N equivalent phase patterns φ_{μ} would achieve the same functionality of φ_F, with 2^N sets of cascaded parameters. To conclude, 2^N distinct functional channels can be achieved. For a simple example of $N = 2$, Fig. 1b shows cascading dual-channel vortex phase patterns to generate four channels of vortex phase patterns. The TCs of the first pattern are $l = +1, +2$ for $|H\rangle$ and $|V\rangle$ input, respectively. While the TCs of the second pattern are $l = -1, +1$, with SEM image of the corresponding metasurface shown in the inset of Fig. 1b. The TCs of four cascaded channels are $l = +1, 0, +3, +2$. Another example of cascading two dual-channel blazed grating patterns to generate four channels of blazed grating patterns is shown in Fig. 1c. The momenta of the first pattern are $(k_x, k_y) = \varepsilon k_0(0,-1), \varepsilon k_0(0,1)$, Where k_0 is the absolute value of wavevector in vacuum, $\varepsilon = 0.01745$ is a constant. While the TCs of the second pattern are $(k_x,k_y) = \varepsilon k_0(1,0),\varepsilon k_0(1,1)$, with SEM image of the corresponding metasurface shown in the inset of Fig. 1c. The momenta of four cascaded channels are $(k_x,k_y) = \varepsilon k_0(1,1),\varepsilon k_0(1,-1),\varepsilon k_0(1,2),\varepsilon k_0(1,0)$.

It should be mentioned that there are no intrinsic cross-talk between channels, since the phase patterns are strictly with the form of φ_F Besides, there are no intrinsic loss since the required Jones matrices of metasurfaces and polarization controllers are all unitary (details can be found in Supplementary Text 1).

Experimental setup

To verify our proposal, a 3-layer setup is implemented for 8-channel switchable wave-front control for certain functionalities. The functionality depends on the designed phase patterns of metasurfaces. Two functionalities of vortex beam generation and beam steering are demonstrated and characterized, respectively. Figure 2a shows a schematic of the optical setup for characterization of vortex beam generation, while Fig. 2b shows that for beam steering. An additional reference light is required for the interference fringes to identify the TC of generated vortex beams, while the deflection direction of beam steering would be characterized with θ and φ in spherical coordinates. Details of the devices and the photograph of the optical setup can be found in Supplementary Text 2.

The metasurfaces are composed of rectangular nanopillar of amorphous silicon (α-Si) on a SiO_2 substrate, and the operation wavelength is considered as 1550 nm. The designed height of nanopillars is 900 nm while the period of arrangement is 800 nm, and the transverse size ranges from 120 nm to 700 nm. Each single metasurface is a square with side length ~640 μm for vortex beam generation, while the side length is ~400 μm for beam steering. Examples of the SEM image of the fabricated metasurfaces are presented in the inset of Fig. 1b, c. The design process of the metasurface can be found in the "Methods" section and Supplementary Text 3, while the fabrication process can be found in the "Methods" section and our previous work[61].

Here, the input polarization state can be either $|H\rangle$ or $|V\rangle$, while $|V\rangle$ is picked up in this work. Liquid-crystal (LC) phase retarders are utilized as the polarization controllers before each metasurface. To electrically switch the input states between $|H\rangle$ and $|V\rangle$, the slow axis of each LC phase retarder is set at 45°. Therefore, for either $|H\rangle$ or $|V\rangle$ input on the LC phase retarder, the state can be varied from one to the other with the phase retardance of π, while the state would keep constant with the phase retardance of 0. By setting appropriate combination of the phase retardance on each LC phase retarder, the input polarization states can be switched among 8 combinations, then the equivalent phase pattern of the whole structure can be switched among 8 channels.

Besides the 3 LC retarders before each metasurface, another LC retarder is settled after the third metasurface so that the output polarization state of each channel is switched back to $|V\rangle$. Finally, the far-field intensity is measured by a CCD camera.

8-channel vortex beam generation

For the vortex beam generation, there is only one target parameter of the TC l. Here, each single metasurface is design as a dual-channel vortex beam generator with the phase pattern form of Eq. 3. It should be mentioned that each phase pattern is additionally overlaid with a blazed grating pattern to separate the generated vortex beam and the zero-order unmodulated light (details in Supplementary Text 4). By cascading LC retarders and 3 metasurfaces with properly designed

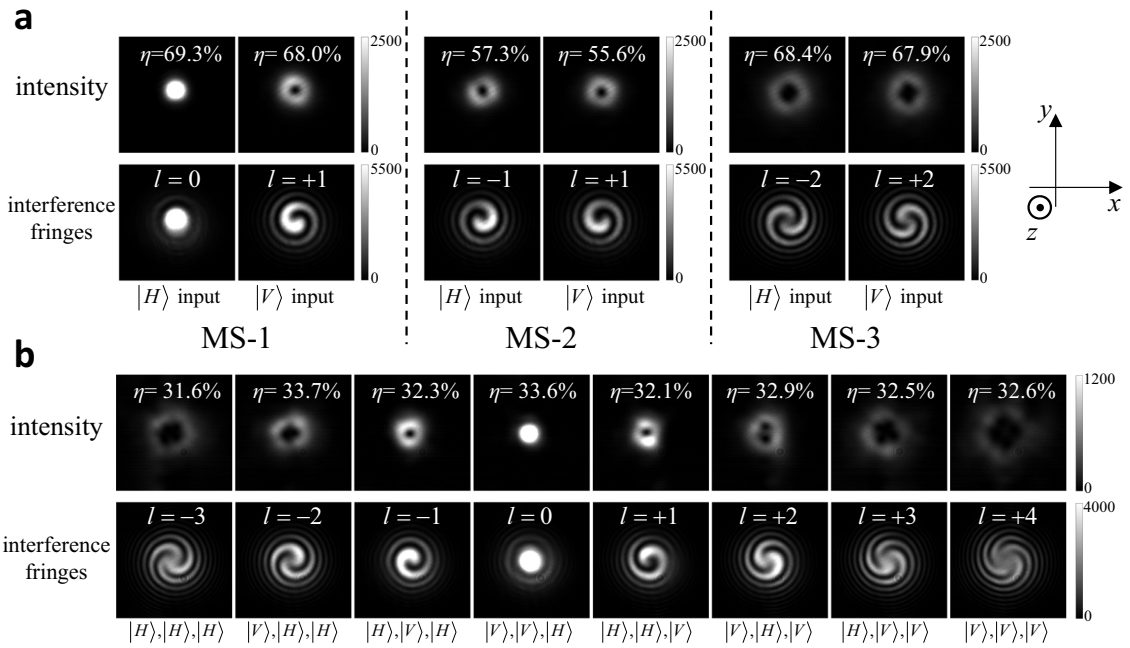

Fig. 3 | Experimental results of 8-channel switchable vortex beam generation. The intensity profiles of generated vortex beams are measured, while the TCs carried by them are characterized by the interference fringes with a fundamental Gaussian mode. **a** Each single metasurface (MS) with $|H\rangle$ and $|V\rangle$ input. The corresponding energy efficiency η is calculated by the total intensity of the beam, and labeled on each intensity profile. **b** 8 channels of cascaded structures, exactly corresponding to 8 combinations of input states of 3 metasurfaces. The corresponding total transmittance η is labeled on each intensity profile. The designed TC l is labeled on each profile of interference fringe. The input states of 3 metasurface are labeled in order below the interference fringe image.

TCs, the TC carried by the generated vortex beam of the whole structure can be switched among 8 pre-determined integer values.

Experimentally, the intensity profiles of generated vortex beams are measured, while the TCs carried by them are characterized by interference fringes with a fundamental Gaussian mode that is aligned to the same polarization state $|V\rangle$. The optical setup is shown in Fig. 2a. First, each single metasurface is characterized with $|H\rangle$ and $|V\rangle$ input, respectively. To characterize a single metasurface, the additional two metasurfaces are removed in Fig. 2a, while the rest elements are fixed. The intensity profiles and corresponding interference fringes are shown in Fig. 3a. The energy efficiency η calculated by the total intensity of each beam is labeled on the intensity profiles, while the designed TC l of each beam is labeled on the profile of interference fringes. Then, each of the 8 channels are characterized by imposing different phase retardance on the LC retarders. The TCs of 8 channels are expected to be the summation of the TCs of each single metasurface for the picked polarization state. For each channel, the intensity profile, total transmittance η, designed TC l, interference fringes, and the specific combination of polarization states are shown in Fig. 3b. As seen in the label of Fig. 3b, the designed TCs of 8 cascaded channels are within the range from $l = -3$ to $l = +4$. To qualitatively observe the TC from the interference fringes, the absolute value of l is determined by the number of spiral arms. While the sign of l is determined by the spiral direction, clockwise for positive and counter-clockwise for negative. As seen in Fig. 3a, b, the TCs of all generated vortex beams agrees well with the design. The energy efficiency of a single layer is within the range from 55.6% to 69.3%, while the total transmittance of the cascaded structure is within the range from 31.6% to 33.7%.

Besides, there can be various TCs of cascaded channels with different settlement of cascading metasurfaces. Another example with the TCs ranging from $l = -1$ to $l = -8$ are experimentally characterized and presented in Supplementary Text 5. Moreover, the interval of TCs can also be varied with non-uniform distribution. A quick example is substituting TCs of the third metasurface with $l = -3, +3$ in Fig. 3a.

8-channel beam steering

There is only one parameter in the aforementioned vortex beam generation. In this section, the functionality of beam steering is further considered as another example with multiple target parameters. In beam steering, the input beam would be deflected. The deflection direction can be varied in a two-dimensional plane, which is determined by two parameters of the transverse momenta along x and y axis, denoted k_x and k_y. To verify our proposal in both one-dimensional and two-dimensional parameter space, two cascaded structures (denoted as A and B) for 8-channel tunable beam steering with different spatial distribution of deflection directions are designed and characterized. Here, each single metasurface is designed for dual-channel beam steering with the phase pattern form of Eq. 4, which can be also regarded as a polarization beam splitter (PBS). The original designed momenta of each single metasurface and both cascaded structures are listed in Table S1 and Table S2.

The samples are experimentally characterized by the far-field deflection directions with a vertically incident beam. The optical set up is shown in Fig. 2b. The camera is moved along z-axis and the deflected beam spot at different distance is recorded, so that the deflection direction of θ and φ in spherical coordinates can be calculated. An example of such measurement with θ and φ labeled is shown on the right of Fig. 2b as well. First, the deflection directions of each single metasurface in cascaded structure A and B are measured and shown in Fig. 4a, c, respectively. As seen in Fig. 4a, c, the first two metasurfaces of both structures are PBSs along y axis. The difference between the two structures is introduced only by the third PBS, which is along y axis in structure A while along x axis in structure B. Then, the deflection directions of all 8 channels of both cascaded structures are measured and shown in Fig. 4b, d, respectively. As seen in Fig. 4b, d, the deflection directions of structure A are arranged in an 8×1 line, while those of B are arranged in a 4×2 grid. Furthermore, the angular errors between measured direction and the original design are plotted in Fig. 4e. It can be seen that the maximum angular error is less than 8′.

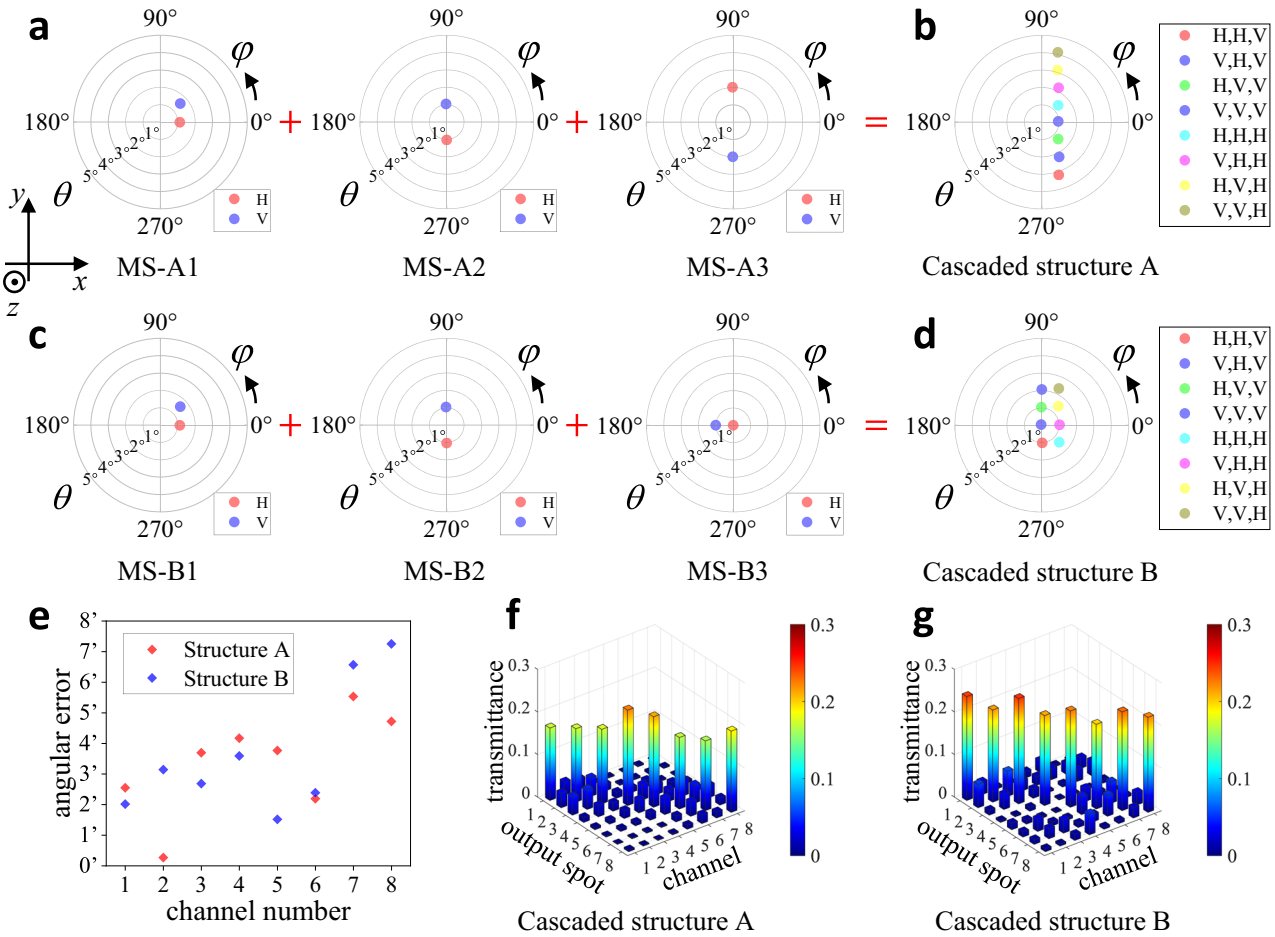

Fig. 4 | Experimental results of 8-channel switchable beam steering. a–d The deflection direction of θ and φ in spherical coordinates measured by the deflected beam spot at different distance. **a** Each single metasurface (MS) in structure A. **b** Cascaded structure A. **c** Each single metasurface in structure B. **d** Cascaded structure B. **e** angular errors between measured deflection direction and the original design. **f**, **g** The transmittance to each deflection direction of each channel. **f** Cascaded structure A. **g** Cascaded structure B.

To characterize the energy efficiency and cross-talk, the transmittance to each deflection direction of each channel is measured and plotted in Fig. 4f, g. For structure A, the transmittance to the main deflection direction is within the range from 15% to 20%, and the cross-talk is below 5% of the input and mainly distributed in adjacent channels. While for structure B, the transmittance is within the range from 20% to 25%, and the cross-talk is more widely distributed. The specific measurement process, original design, and raw data can be found in Supplementary Text 6. Although the current maximum deflection angle is about 4°, it can be extended by cascading metasurfaces with larger deflection angles (detailed discussions can be found in Supplementary Text 7).

Discussion

In the operation principle of our proposal, the whole phase pattern is supposed to be simply the summation of each single phase pattern, without considering the propagation between metasurfaces. In the present work, this is guaranteed by employing a 4-*f* system between each pair of adjacent metasurfaces, so that the input field of the second one can be identical with the output field of the first one (rotated 180° along *z* axis). Actually, such 4-*f* systems are not necessary, since the effect of propagation can be ignored or compensated if the distance between metasurfaces is less than several millimeters. This is possible by closely attaching metasurfaces and thinner LC retarders as a compact module[49,62,63]. Moreover, metasurfaces can be integrated with LCs[64]. Thus, it is potential to achieve a fully integrated module while retaining the advantage of low thickness as a single metasurface and the detailed discussions are provided in Supplementary Text 8. Besides, the number of electrodes required for electrically switching is determined by LC retarders and almost equal to the layers. Therefore, the design and fabrication of electrode are significantly simpler than pixel-by-pixel electro-optical reconfigurable metasurfaces[27], where the number of electrodes is equal to those of the pixels.

It should be mentioned that there are some reported methods of metasurface design to achieve complex amplitude control[51,65] or Jones matrix with non-diagonal elements[52,56,57]. With such metasurfaces, the cascaded structure would be potential to achieve much more functionalities. However, the main problem is that there would be intrinsic loss, which is introduced by the amplitude manipulation. For the multiple-layer cascaded structure in our proposal, the loss would accumulate and significantly affect the final efficiency. Thus, in this work, the metasurfaces are restricted to phase-only patterns to avoid intrinsic loss.

Although there are no intrinsic loss or cross-talk, the experimental efficiency per layer is 40–70% and the cross-talk per layer is 3–5% in the present work. As the cascaded layers increases, the stray light, cross-talk, and loss would also accumulate and become unacceptable. However, they are all introduced by the non-ideal factors in metasurface design and fabrication. For example, there would be unmodulated light of metasurface[66–68]. In the vortex beam generation of this work, a blazed grating pattern is overlaid on the phase pattern to spatially separate the unmodulated light[69], and details are presented in Supplementary Text 4. These non-ideal factors can be further reduced

with improved design approach of metasurfaces, e.g., inverse design[70–74] or adjoint optimization[75,76], thus the accumulated stray light, cross-talk and loss with increased cascading layers can be within control. These methods go beyond the present work, but we have been engaged in related researches.

To conclude, we have achieved 2^N electrically switchable channels for certain functionalities with N cascaded metasurfaces combined with LC phase retarders. Although the condition is that the phase pattern of cascaded structure should have the same function form with that of a single metasurface, some common dynamic wave-front controlled functionalities can be covered, including beam steering, vortex beam generation, lens, etc. Moreover, our proposal can be extended to other materials, frequencies, and metasurface design approaches. Thus, it is potential to be applied on LiDAR, glasses-free 3D display, OAM (de)multiplexing, and varifocal meta-lens. With more enough channels and richer functionalities, we believe our work would provide a practical way towards metasurfaces with tunable functionalities.

Methods

Numerical Simulation

The amplitude and phase modulation of rectangular nanopillars with different height, period, length and width are numerically calculated by the Finite Difference Time Domain (FDTD) method. For the eventually used set, the height is 900 nm while the period is 800 nm, and the transverse size ranges from 120 nm to 700 nm. The detailed simulation and design process of the metasurface can be found in Supplementary Text 3.

Fabrication

First, 900nm-thick α-Si is deposited on a quartz substrate by PECVD. Then, a layer of Cr as metal hard mask are deposited by electron beam (EB) evaporation, and a layer of SiO_2 is grown on the Cr layer as an additional hard mask to avoid experimentally uncontrollable lift-off process of Cr. After that, the rectangular patterns are fabricated by EB lithography and inductively coupled plasma reactive ion etching (ICP-RIE). The detailed fabrication process are similar to that of our previous work[61].

Data availability

All the processed data of this work are provided within the main text and supplementary materials. The raw data are available from the corresponding author upon request.

Code availability

The codes used for simulation, design and data process are available from the corresponding author upon request.

References

1. Yu, N. et al. Light propagation with phase discontinuities: generalized laws of reflection and refraction. *Science* **334**, 333–337 (2011).
2. Lin, D., Fan, P., Hasman, E. & Brongersma, M. L. Dielectric gradient metasurface optical elements. *Science* **345**, 298–302 (2014).
3. Liu, L. et al. Broadband metasurfaces with simultaneous control of phase and amplitude. *Adv. Mater.* **26**, 5031–5036 (2014).
4. Ren, H. et al. Complex-amplitude metasurface-based orbital angular momentum holography in momentum space. *Nat. Nanotechnol.* **15**, 948–955 (2020).
5. Overvig, A. C. et al. Dielectric metasurfaces for complete and independent control of the optical amplitude and phase. *Light Sci. Appl* **8**, 92 (2019).
6. Yang, Y. et al. Dielectric meta-reflectarray for broadband linear polarization conversion and optical vortex generation. *Nano Lett.* **14**, 1394–1399 (2014).
7. Arbabi, A., Horie, Y., Bagheri, M. & Faraon, A. Dielectric metasurfaces for complete control of phase and polarization with subwavelength spatial resolution and high transmission. *Nat. Nanotech* **10**, 937–943 (2015).
8. Nookala, N. et al. Ultrathin gradient nonlinear metasurface with a giant nonlinear response. *Optica* **3**, 283 (2016).
9. Ye, W. et al. Spin and wavelength multiplexed nonlinear metasurface holography. *Nat. Commun.* **7**, 11930 (2016).
10. Zhao, Y., Belkin, M. A. & Alù, A. Twisted optical metamaterials for planarized ultrathin broadband circular polarizers. *Nat. Commun.* **3**, 870 (2012).
11. Akram, M. R., Ding, G., Chen, K., Feng, Y. & Zhu, W. Ultrathin single layer metasurfaces with ultra-wideband operation for both transmission and reflection. *Adv. Mater.* **32**, 1907308 (2020).
12. Conteduca, D. et al. Dielectric nanohole array metasurface for high-resolution near-field sensing and imaging. *Nat. Commun.* **12**, 3293 (2021).
13. Xu, J. et al. Wide-angular-range and high-resolution beam steering by a metasurface-coupled phased array. *Opt. Lett.* **43**, 5255 (2018).
14. Zheng, G. et al. Metasurface holograms reaching 80% efficiency. *Nat. Nanotech* **10**, 308–312 (2015).
15. Shalaev, M. I. et al. High-efficiency all-dielectric metasurfaces for ultracompact beam manipulation in transmission mode. *Nano Lett.* **15**, 6261–6266 (2015).
16. Deng, Y., Wu, C., Meng, C., Bozhevolnyi, S. I. & Ding, F. Functional metasurface quarter-wave plates for simultaneous polarization conversion and beam steering. *ACS Nano* **15**, 18532–18540 (2021).
17. He, F., MacDonald, K. F. & Fang, X. Continuous beam steering by coherent light-by-light control of dielectric metasurface phase gradient. *Opt. Express* **28**, 30107 (2020).
18. Wei, Z. et al. Highly efficient beam steering with a transparent metasurface. *Opt. Express* **21**, 10739 (2013).
19. Wang, S. et al. A broadband achromatic metalens in the visible. *Nat. Nanotech* **13**, 227–232 (2018).
20. Paniagua-Domínguez, R. et al. A Metalens with a Near-Unity Numerical Aperture. *Nano Lett.* **18**, 2124–2132 (2018).
21. Bouchard, F. et al. Optical spin-to-orbital angular momentum conversion in ultra-thin metasurfaces with arbitrary topological charges. *Appl. Phys. Lett.* **105**, 101905 (2014).
22. Ni, X., Kildishev, A. V. & Shalaev, V. M. Metasurface holograms for visible light. *Nat. Commun.* **4**, 2807 (2013).
23. Huang, K. et al. Ultrahigh-capacity non-periodic photon sieves operating in visible light. *Nat. Commun.* **6**, 7059 (2015).
24. Park, J. et al. All-solid-state spatial light modulator with independent phase and amplitude control for three-dimensional LiDAR applications. *Nat. Nanotechnol.* **16**, 69–76 (2021).
25. Li, L. et al. Electromagnetic reprogrammable coding-metasurface holograms. *Nat. Commun.* **8**, 197 (2017).
26. Sherrott, M. C. et al. Experimental demonstration of >230° phase modulation in gate-tunable graphene–gold reconfigurable mid-infrared metasurfaces. *Nano Lett.* **17**, 3027–3034 (2017).
27. Kim, S. I. et al. Two-dimensional beam steering with tunable metasurface in infrared regime. *Nanophotonics* **11**, 2719–2726 (2022).
28. Arbabi, E. et al. MEMS-tunable dielectric metasurface lens. *Nat. Commun.* **9**, 812 (2018).
29. Gutruf, P. et al. Mechanically tunable dielectric resonator metasurfaces at visible frequencies. *ACS Nano* **10**, 133–141 (2016).
30. Ee, H.-S. & Agarwal, R. Tunable metasurface and flat optical zoom lens on a stretchable substrate. *Nano Lett.* **16**, 2818–2823 (2016).
31. Chu, C. H. et al. Active dielectric metasurface based on phase-change medium. *Laser Photonics Rev.* **10**, 986–994 (2016).
32. Zhu, Z., Evans, P. G., Haglund, R. F. & Valentine, J. G. Dynamically reconfigurable metadevice employing nanostructured phase-change materials. *Nano Lett.* **17**, 4881–4885 (2017).
33. Dorrah, A. H. & Capasso, F. Tunable structured light with flat optics. *Science* **376**, eabi6860 (2022).

34. Leitis, A. et al. Angle-multiplexed all-dielectric metasurfaces for broadband molecular fingerprint retrieval. *Sci. Adv.* **5**, eaaw2871 (2019).
35. Wan, S. et al. Angular-multiplexing metasurface: building up independent-encoded amplitude/phase dictionary for angular illumination. *Adv. Optical Mater.* **9**, 2101547 (2021).
36. Chen, K. et al. Directional janus metasurface. *Adv. Mater.* **32**, 1906352 (2020).
37. Chen, Y., Yang, X. & Gao, J. 3D Janus plasmonic helical nanoapertures for polarization-encrypted data storage. *Light Sci. Appl.* **8**, 45 (2019).
38. Zhou, Y. et al. Multifunctional metaoptics based on bilayer metasurfaces. *Light Sci. Appl.* **8**, 80 (2019).
39. Shi, Z. et al. Single-layer metasurface with controllable multiwavelength functions. *Nano Lett.* **18**, 2420–2427 (2018).
40. Wang, B. et al. Visible-frequency dielectric metasurfaces for multiwavelength achromatic and highly dispersive holograms. *Nano Lett.* **16**, 5235–5240 (2016).
41. Xu, H. et al. Wavevector and frequency multiplexing performed by a spin-decoupled multichannel metasurface. *Adv. Mater. Technol.* **5**, 1900710 (2020).
42. Ren, H. et al. Metasurface orbital angular momentum holography. *Nat. Commun.* **10**, 2986 (2019).
43. Yang, H. et al. Angular momentum holography via a minimalist metasurface for optical nested encryption. *Light Sci. Appl* **12**, 79 (2023).
44. Zhang, L. et al. Highly tunable cascaded metasurfaces for continuous two-dimensional beam steering. *Adv. Sci.* **10**, 2300542 (2023).
45. Wang, E. W., Yu, S., Phan, T., Dhuey, S. & Fan, J. A. Arbitrary achromatic polarization control with reconfigurable metasurface systems. *Laser Photonics Rev.* **17**, 2200926 (2023).
46. Zhang, X. et al. Switchable diffraction pattern based on cascaded metasurfaces. *Laser Photonics Rev.* 2300887 https://doi.org/10.1002/lpor.202300887 (2024).
47. Wei, Q. et al. Rotational multiplexing method based on cascaded metasurface holography. *Adv. Opt. Mater.* **10**, 2102166 (2022).
48. Ogawa, C., Nakamura, S., Aso, T., Ikezawa, S. & Iwami, K. Rotational varifocal moiré metalens made of single-crystal silicon meta-atoms for visible wavelengths. *Nanophotonics* **11**, 1941–1948 (2022).
49. Badloe, T., Kim, I., Kim, Y., Kim, J. & Rho, J. Electrically tunable bifocal metalens with diffraction-limited focusing and imaging at visible wavelengths. *Adv. Sci.* **8**, 2102646 (2021).
50. Devlin, R. C., Ambrosio, A., Rubin, N. A., Mueller, J. P. B. & Capasso, F. Arbitrary spin-to–orbital angular momentum conversion of light. *Science* **358**, 896–901 (2017).
51. Liu, M. et al. Multifunctional metasurfaces enabled by simultaneous and independent control of phase and amplitude for orthogonal polarization states. *Light Sci. Appl.* **10**, 107 (2021).
52. Rubin, N. A., Zaidi, A., Dorrah, A. H., Shi, Z. & Capasso, F. Jones matrix holography with metasurfaces. *Sci. Adv.* **7**, eabg7488 (2021).
53. Rubin, N. A., Shi, Z. & Capasso, F. Polarization in diffractive optics and metasurfaces. *Adv. Opt. Photonics* **13**, 836 (2021).
54. Ou, X. et al. Tunable polarization-multiplexed achromatic dielectric metalens. *Nano Lett.* **22**, 10049–10056 (2022).
55. Liu, M. et al. Broadband generation of perfect Poincaré beams via dielectric spin-multiplexed metasurface. *Nat. Commun.* **12**, 2230 (2021).
56. Bao, Y., Wen, L., Chen, Q., Qiu, C.-W. & Li, B. Toward the capacity limit of 2D planar Jones matrix with a single-layer metasurface. *Sci. Adv.* **7**, eabh0365 (2021).
57. Xiong, B. et al. Breaking the limitation of polarization multiplexing in optical metasurfaces with engineered noise. *Science* **379**, 294–299 (2023).
58. Lian, Y. et al. OAM beam generation in space and its applications: a review. *Opt. Lasers Eng.* **151**, 106923 (2022).
59. Bryngdahl, O. Formation of blazed gratings. *J. Opt. Soc. Am.* **60**, 140_1 (1970).
60. Goodman, J. W. & Cox, M. E. Introduction to Fourier optics. *Phys. Today* **22**, 97–101 (1969).
61. Tian, T. et al. Metasurface-based free-space multi-port beam splitter with arbitrary power ratio. *Adv. Opt. Mater.* **11**, 2300664 (2023).
62. Kim, I. et al. Stimuli-responsive dynamic metaholographic displays with designer liquid crystal modulators. *Adv. Mater.* **32**, 2004664 (2020).
63. Kim, I. et al. Pixelated bifunctional metasurface-driven dynamic vectorial holographic color prints for photonic security platform. *Nat. Commun.* **12**, 3614 (2021).
64. Hu, Y. et al. Electrically tunable multifunctional polarization-dependent metasurfaces integrated with liquid crystals in the visible region. *Nano Lett.* **21**, 4554–4562 (2021).
65. Fan, Q. et al. Independent amplitude control of arbitrary orthogonal states of polarization via dielectric metasurfaces. *Phys. Rev. Lett.* **125**, 267402 (2020).
66. Wang, J. et al. All-dielectric metasurface grating for on-chip multichannel orbital angular momentum generation and detection. *Opt. Express* **27**, 18794 (2019).
67. Lim, K. T. P., Liu, H., Liu, Y. & Yang, J. K. W. Holographic colour prints for enhanced optical security by combined phase and amplitude control. *Nat. Commun.* **10**, 25 (2019).
68. Balthasar Mueller, J. P., Rubin, N. A., Devlin, R. C., Groever, B. & Capasso, F. Metasurface polarization optics: independent phase control of arbitrary orthogonal states of polarization. *Phys. Rev. Lett.* **118**, 113901 (2017).
69. Padgett, M. & Di Leonardo, R. Holographic optical tweezers and their relevance to lab on chip devices. *Lab Chip* **11**, 1196 (2011).
70. Zheng, Y. et al. Designing high-efficiency extended depth-of-focus metalens via topology-shape optimization. *Nanophotonics* **11**, 2967–2975 (2022).
71. Hadibrata, W., Wei, H., Krishnaswamy, S. & Aydin, K. Inverse design and 3D printing of a metalens on an optical fiber tip for direct laser lithography. *Nano Lett.* **21**, 2422–2428 (2021).
72. Li, Z. et al. Inverse design enables large-scale high-performance meta-optics reshaping virtual reality. *Nat. Commun.* **13**, 2409 (2022).
73. Schubert, M. F., Cheung, A. K. C., Williamson, I. A. D., Spyra, A. & Alexander, D. H. Inverse design of photonic devices with strict foundry fabrication constraints. *ACS Photonics* **9**, 2327–2336 (2022).
74. Ahn, G. H. et al. Photonic inverse design of on-chip microresonators. *ACS Photonics* **9**, 1875–1881 (2022).
75. Zhou, M. et al. Inverse design of metasurfaces based on coupled-mode theory and adjoint optimization. *ACS Photonics* **8**, 2265–2273 (2021).
76. Mansouree, M., McClung, A., Samudrala, S. & Arbabi, A. Large-scale parametrized metasurface design using adjoint optimization. *ACS Photonics* **8**, 455–463 (2021).

Acknowledgements

Funding from the National Key Research and Development Program of China (Grant No. 2023YFB2806703) received by Y.H., the National Natural Science Foundation of China (Grant No. U22A6004) received by Y.H. and the National Natural Science Foundation of China (Grant No. 92365210) received by W.Z. is greatly acknowledged. This work was also supported by the project of Tsinghua University-Zhuhai Huafa Industrial Share Company Joint Institute for Architecture Optoelectronic Technologies (JIAOT), Beijing National Research Center for Information Science and Technology (BNRist), Frontier Science Center for Quantum Information, Beijing academy of quantum information science, and Tsinghua University Initiative Scientific Research Program. The authors would like to thank Zhe Li, Deyang Kong, and Jiahao Tian for their valuable discussions and helpful comments.

Author contributions

Z.M. and X.F. conceived the idea. Z.M. theoretically verified the principle, designed and performed the simulations, experiments and data analysis. T.T. contributed significantly to the fabrication process. Y.Liao contributed to the numerical simulations. Y.Li, K.C., F.L, H.S., and W.Z. provided useful discussions and comments. Z.M. and X.F. wrote the paper. Y.H. revised the manuscript. All authors approved the manuscript.

Competing interests

The authors declare no competing interests.

Additional information

Supplementary information The online version contains supplementary material available at https://doi.org/10.1038/s41467-024-52676-w.

Correspondence and requests for materials should be addressed to Xue Feng or Yidong Huang.

Peer review information *Nature Communications* thanks Shumin Xiao and Ting Xu for their contribution to the peer review of this work. A peer review file is available.